Available online at www.sciencedirect.com
ScienceDirect
Applied Catalysis B: Environmental 83 (2008) 240–255
APPLIED CATALYSIS B: ENVIRONMENTAL
www.elsevier.com/locate/apcatb

Au/$Ce_{1-x}Zr_xO_2$ as effective catalysts for low-temperature CO oxidation

Izabela Dobrosz-Gómez [1], Ireneusz Kocemba, Jacek M. Rynkowski *

Institute of General and Ecological Chemistry, Technical University of Łódź, 90-924 Łódź, Żeromskiego 116, Poland

Received 13 November 2007; received in revised form 26 January 2008; accepted 4 February 2008
Available online 20 February 2008

Abstract

The physico-chemical properties and activity of Ce-Zr mixed oxides, CeO_2 and ZrO_2 in CO oxidation have been studied considering both their usefulness as supports for Au nanoparticles and their contribution to the reaction. A series of $Ce_{1-x}Zr_xO_2$ ($x = 0$, 0.25, 0.5, 0.75, 1) oxides has been prepared by sol–gel like method and tested in CO oxidation. Highly uniform, nanosized, Ce-Zr solid solutions were obtained. The activity of mixed oxides in CO oxidation was found to be dependent on Ce/Zr molar ratio and related to their reducibility and/or oxygen mobility. CeO_2 and $Ce_{0.75}Zr_{0.25}O_2$, characterized by the cubic crystalline phase show the highest activity in CO oxidation. It suggests that the presence of a cubic crystalline phase in Ce-Zr solid solution improves its catalytic activity in CO oxidation. The relation between the physico-chemical properties of the supports and the catalytic performance of Au/$Ce_{1-x}Zr_xO_2$ catalysts in CO oxidation reaction has been investigated. Gold was deposited by the direct anionic exchange (DAE) method. The role of the support in the creation of catalytic performance of supported Au nanoparticles in CO oxidation was significant. A direct correlation between activity and catalysts reducibility was observed. Ceria, which is susceptible to the reduction at the lowest temperature, in the presence of highly dispersed Au nanoparticles, appears to be responsible for the activity of the studied catalysts. CeO_2-ZrO_2 mixed oxides are promising supports for Au nanoparticles in CO oxidation whose activity is found to be dependent on Ce/Zr molar ratio.

Keywords: Au; Ce-Zr mixed oxide; Gold catalyst; CO oxidation

1. Introduction

Catalytic oxidation of CO is one of important reactions due to its relevance in practical applications such as purification of breathing air in closed spaces, safety masks, gas sensors for the detection of trace amounts of CO in air, closed-cycle CO_2 lasers, automotive exhaust treatments, etc. The possibility of using supported gold nanoparticles as efficient catalysts for low-temperature reactions has aroused a lot of interest since the pioneering work of Haruta et al. [1] which showed the high activity of gold deposited on various metal oxides towards CO oxidation. Then several research groups confirmed that low-temperature CO oxidation is successfully catalysed by gold nanoparticles highly dispersed on partly reducible oxides [2–7]. Consequently, there is a strong interest in developing gold catalysts with high oxidation activity at low temperatures.

In recent years, gold deposited on different materials, among them cerium and zirconium oxides have become a subject of many papers [8,9]. Both Au/CeO_2 and Au/ZrO_2 systems are considered as promising catalysts for low-temperature CO oxidation [10–13]. Most recently, Sun et al. [14] and Chang et al. [15] have reported a very high activity of Au/CeO_2 catalysts for CO oxidation in air at room temperature. Russo et al. [8] have studied the activity of Au/CeO_2 and Au/ZrO_2 catalysts prepared by the innovative combustion synthesis method in CO oxidation. However, from their results, those systems are not active at temperatures below 150 °C. On the other hand, Au/ZrO_2 catalysts prepared by deposition–precipitation method have been described as active catalysts for CO oxidation in air both at room temperature and below 0 °C, as reported by Konova et al. [16] and Wolf and Schüth [17], respectively.

The growing interest in studies of the catalytic activity of gold supported on some transition metal oxides can be seen for the last 25 years [18–23]. The efficiency of supported gold nanoparticles in CO oxidation at low temperature depends on various factors including, e.g., the size and shape of Au

[1] Present address: Facultad de Ciencias Exactas y Naturales, Universidad Nacional de Colombia, Sede Manizales.
[1] Present address: Facultad de Ciencias Exactas y Naturales, Universidad Nacional de Colombia, Sede Manizales.

0926-3373/$ – see front matter © 2008 Elsevier B.V. All rights reserved.
doi:10.1016/j.apcatb.2008.02.012

particles, preparation procedures, pretreatment conditions [24–26]. Beside these factors, the support importance in the creation of their catalytic performance must be emphasized. The role of the support in the stabilization of the active phase dispersion and modification of its electronic state is significant and well known [3,27,28]. According to literature [29–31] it can also play a role in the activation of reactants, especially oxygen. However, many questions concerning especially the reaction mechanism and the role of the oxide support remain still not clear.

In order to understand the relation between the support properties and catalytic performance of supported Au nanoparticles, Ce-Zr mixed oxides, CeO_2 and ZrO_2 as supports for Au were used. One of the arguments that drove us to select Ce-Zr mixed oxides was their unique redox properties and high mobility of lattice oxygen. These properties strongly depend on Ce/Zr molar ratio. Furthermore, ceria is known to be active for the removal of post-combustion pollutants [32]. Moreover, in the last generation of commercial three-way catalysts (TWCs), better catalytic performance can be obtained when the supports contain ceria-zirconia solid solutions instead of pure CeO_2, as reported by Daturi et al. [33]. Also, similar value of the isoelectric point (IEP) for CeO_2, ZrO_2 and their mixed oxides, allow us to create comparable conditions for gold deposition. So far, CeO_2-ZrO_2 systems have been widely investigated in many applications [34]. However, only few papers have reported the study of Au supported on ceria-zirconia as catalysts for CO oxidation [35,36].

Furthermore, gold nanoparticles dispersed on different mixed oxide supports, such as Cu-Mg-Al-O [37] CeO_2-Al_2O_3 [38], Ce-Ti-O [39], CuO-CeO_2 [40], Au/$La_{1-x}Sr_xMnO_3$ and Au/$La_{1-x}Sr_xCrO_3$ composites [41] and $MgAl_2O_4$ spinel monoliths [42] are recently a subject of big interest due to their high activity in numerous reactions, among them CO oxidation.

The aim of this work is to understand the relation between the physico-chemical properties of the supports and the catalytic performance of Au/$Ce_{1-x}Zr_xO_2$ catalysts in CO oxidation reaction. The usefulness of CeO_2-ZrO_2 mixed oxides, CeO_2 and ZrO_2 as supports for Au nanoparticles has been studied, from the point of view of their contribution to the reaction. The $Ce_{1-x}Zr_xO_2$ (x = 0, 0.25, 0.5, 0.75, 1) oxides and Au/$Ce_{1-x}Zr_xO_2$ catalysts were synthesized, characterized by BET, SEM-EDS, X-ray diffraction (XRD), Temperature Programmed Reduction (TPR-CO), High-Resolution Transmission Electron Microscopy (HRTEM), Atomic Absorption Spectroscopy (AAS), and tested in CO oxidation under stationary conditions.

2. Experimental

2.1. Synthesis

A series of $Ce_{1-x}Zr_xO_2$ (x = 0.25, 0.5, 0.75) solid solutions, CeO_2 and ZrO_2 was prepared by the sol–gel like method, based on a thermal decomposition of mixed propionates [43]. The starting materials, zirconium(IV) acetylacetonate [$Zr(CH_3COCH_2COCH_3)_4$, Avocado] and/or cerium(III) acetyloacetonate hydrate [$Ce(CH_3COCH_2COCH_3)_3{\cdot}H_2O$, Sigma–Aldrich] were dissolved in boiling propionic acid in concentration of 0.12 M. Boiling solutions were mixed and the solvent was evaporated until a resin was obtained. All samples were calcined in air at 550 °C for 4 h.

Hydrogen tetrachloroaureate(III) trihydrate [$HAuCl_4{\cdot}3H_2O$, Sigma–Aldrich] was used as a gold precursor. The catalysts were prepared by the direct anionic exchange (DAE) method of gold species with hydroxyl groups of the support [25,44]. The optimisation of catalyst synthesis conditions was presented previously [45]. Aqueous solutions of $HAuCl_4$ at the concentration 2.25×10^{-4} M were prepared using 900 cm^3 of distilled water. The solution was heated up to 70 °C and the support was introduced. After 1 h of thermostating and vigorous stirring, the suspension was centrifuged. In order to remove the residual chlorine from the catalysts, the obtained solid was suspended in 4 M ammonia solution, stirred for 1 h and next centrifuged again. After drying in an oven at 120 °C overnight, the catalysts were calcined in air at 300 °C for 4 h.

2.2. Characterization methods

Nitrogen adsorption/desorption isotherms at −196 °C were measured using Sorptomatic 1900 apparatus (Carlo-Erba). Prior to the measurement, all samples were degassed for 4 h at 250 °C. The specific surface area, S_{BET} was calculated using BET equation.

Scanning electron microscopy (SEM) measurements were performed by S-4700 microscope (Hitachi, Japan) [46], using an acceleration voltage 20 kV, equipped with energy dispersive spectrometer (EDS) (Thermo Noran, USA). Images were recorded at several magnifications. The application of the EDS method allowed determining the content of elements in the studied microarea of the investigated oxides and catalysts, based on the obtained characteristic X-ray spectra. An attempt to estimate the dispersion of Au was undertaken using the images recorded with the back-scattered electron (BSE) YAG-type detector. The investigated samples were placed in a holder and before analysing were coated with a carbon monolayer in order to reduce the charge buildup on the samples.

X-ray diffraction patterns were obtained at room temperature using a PANalytical X'Pert Pro MPD diffractometer, operating at 40 kV and 30 mA (Cu Kα radiation). Data were collected in the range 20–80° 2θ with a step size of 0.0167° and step time of 10 s. JCPDS files were used for the identification of the diffraction peaks. Approximately 300 mg of sample, which had been hand ground in an agate mortar, was packed in the sample holder. The particle size was estimated from the width of principal diffraction peaks using the Scherrer equation.

The "a" lattice constant was calculated from the cubic root of normalized volume of sample by using the u-fit software. This parameter corresponds to the width of a unitary net of catalyst in the cubic system.

Temperature Programmed Reduction (TPR-CO) experiments were carried out by PEAK-4 apparatus [47], using CO as reducing agent. The apparatus was equipped with an infrared gas analyser (Fuji Electric Systems Co., type: ZRJ-4) to analyse

CO_2 formation. TPR-CO experiments were performed using a CO/He (5 vol.% CO, 95 vol.% He) gas mixture, with a flow rate of 40 $cm^3\ min^{-1}$, in the temperature range 25–850 °C, with a ramp rate 15 °C min^{-1}. Powdered samples of 100 mg were exposed to dry Ar at 250 °C for 1 h before the reduction. Based on the CO_2 formation, reduction degrees of the investigated oxides were calculated. The reduction of NiO to metallic Ni, according to the reaction: $NiO + CO \rightarrow Ni + CO_2$, as a standard to calibrate the CO_2 formation was used. As the first step of the calibration, the surface area under the TPR-CO profile for NiO reduction was estimated. The obtained value responded to the theoretical quantity of the reducing agent used during the process. For the tested samples CO consumption was estimated using the following equation:

$$\mathrm{CO}\,(\mathrm{mmol\,g^{-1}}) = (S_{\mathrm{oxide}}/m_{\mathrm{oxide}}) \times (m_{\mathrm{NiO}}/S_{\mathrm{NiO}}) \times (1000/74.69) \quad (1)$$

where S_{oxide}, S_{NiO} correspond to the surface area under the TPR profile for the investigated oxide and NiO, respectively; m_{oxide}, m_{NiO} correspond to the sample weight of the oxide and NiO, respectively; 74.69—NiO molar weight (g mol^{-1}).

Atomic Absorption Spectroscopy analyses were performed with a Solaar M6 Unicam spectrophotometer in order to estimate an amount of Au deposited on supports. Initially, the microwave digestions of the analysed samples were performed by aqua regia (3 cm^3 + 100 mg of the sample), using microwave oven MLS-1200 MEGA (Milestone). The obtained solutions were placed in measuring flasks and diluted with 100 cm^3 of deionised water. A blank test was prepared in the similar way.

High-Resolution Transmission Electron Microscopy measurements were carried out using high-resolution microscopes EM-002B (TOPCON 200 kV) and JEOL-JEM 200CX at 10^{-5} Pa to determine the gold particle size distribution. For analysis, samples were placed on a Cu-mesh. The identification of Au particles was performed by SAED-selected area electron diffraction on bright and dark fields. The mean particle diameters were calculated, as described previously [25].

CO oxidation reaction was carried out at atmospheric pressure in a quartz flow microreactor containing 100 mg of sample in a fixed bed, using a series of mass flow controllers with diluted gases. Before the reaction, a pretreatment in air at 300 °C (for the catalysts) and 550 °C (for the oxide supports) for 1 h with a ramp rate of 5 °C min^{-1} was carried out. Three different gas mixture containing 1.7 vol.% CO and 3.4 vol.% O_2, 3.4 vol.% CO and 1.7 vol.% O_2 or 4.1 vol.% CO and 1.0 vol.% O_2 (He as an eluant gas) were used with a flow of 50 $cm^3\ min^{-1}$, in the temperature range 25–300 °C (for the catalysts) or 25–550 °C (for the oxide supports), with a ramp rate 5 °C min^{-1}. The catalytic experiments were repeated several times in order to verify their reproducibility. Gas chromatograph fitted with molecular sieves 5 Å, equipped with a thermal conductivity detector was used to perform the analysis of both CO and O_2 concentration. The CO conversion was calculated, as described previously [35]. The catalytic performance of materials was assessed in terms of both T_{10} and T_{50} temperatures, defined as the temperature when 10 and 50% conversion was obtained, respectively.

The catalytic tests at 0 °C as well as at temperatures below 0 °C were carried out using a CO/air (0.24 vol.% CO, 99.76 vol.% air) gas mixture, employing an infrared gas analyser (Fuji Electric Systems Co., type: ZRJ-4) to analyse CO_2 formation. Before the reaction, a pretreatment in air at 300 °C for 1 h with a ramp rate of 5 °C min^{-1} was carried out. The oxidation tests were conducted at atmospheric pressure in a quartz flow U-shape microreactor containing 100 mg of catalyst in a fixed bed, immersed in appropriate freezing mixture, with a flow rate of 50 $cm^3\ min^{-1}$, in the temperature range −55 to 25 °C. Depending on the expected temperature, at which CO oxidation reactions were carried out, different freezing mixtures were used.

3. Results and discussion

3.1. The characterization of ceria, zirconia and ceria-zirconia supports

3.1.1. Textural and morphological characterization

The surface areas of the oxides used as supports for Au in this study were determined by N_2 BET method (Table 1). CeO_2 shows the highest surface area (ca. 58 $m^2\ g^{-1}$). However, for ZrO_2 prepared in a similar way, the observed surface area is very low (ca. 4.5 $m^2\ g^{-1}$). Under similar synthesis conditions of the binary oxides, a slight effect of the sample composition on its surface area is observed. The substitution of cerium by an increasing amount of zirconium slightly decreases their surface area from ca. 50 to ca. 41 $m^2\ g^{-1}$ for $Ce_{0.75}Zr_{0.25}O_2$ and $Ce_{0.25}Zr_{0.75}O_2$, respectively. These data are related to textural properties of the oxides, as discussed below.

The morphology of some powders calcined at 550 °C is illustrated in Fig. 1 with some representative SEM micrographs.

The results show that the oxides prepared by the sol–gel method are highly uniform. The effect of the composition on their morphology can be observed. For CeO_2, both the size and shape of particles suggest the presence of aggregates of spherical grains of dimension lower than 1 μm. In the case of $Ce_{0.75}Zr_{0.25}O_2$, the agglomeration of regular and plated shaped particles is found. However, for ZrO_2 typical angular and faced large particles with a characteristic structure evident at 5 μm magnification are observed. As far as the porosity of the oxides is concerned, the micrographs at this magnification reveal the presence of porosity in the submicrometer range in CeO_2 which is absent in pure ZrO_2 and $Ce_{0.75}Zr_{0.25}O_2$. The application of the EDS method allow to determine the content of elements in the studied microarea of the oxide surface layer based on the obtained characteristic X-ray spectra, as presented in Fig. 1.

The phases present in $Ce_{1-x}Zr_xO_2$ (x = 0, 0.25, 0.5, 0.75, 1) oxides were established by XRD and results are presented in Fig. 2. Crystalline phases were identified by a comparison with the corresponding JCPDS files. XRD pattern of CeO_2 corresponds to a single cubic phase, fluorite-type structure (JCPDS: 03-065-2975) and that of ZrO_2 corresponds to both

Table 1
Characterization of $Ce_{1-x}Zr_xO_2$ oxides calcined at 550 °C

Oxide composition	Lattice type[a]	Lattice parameters values[a] (Å)	The average crystallites size[a] (nm)	Surface area[b] ($m^2\ g^{-1}$)
CeO_2	Cubic *Fm3m*	$a = 5.4112$	14.2 Ce(1 1 1)	58.1
$Ce_{0.75}Zr_{0.25}O_2$	Cubic *Fm3m*	$a = 5.3490$	7.0 Ce(1 1 1)	50.1
$Ce_{0.5}Zr_{0.5}O_2$	Tetragonal *P42/nmc*	$a = 3.6678$ $c = 5.3039$	6.4 Ce(1 0 1)	46.5
$Ce_{0.25}Zr_{0.75}O_2$	Tetragonal *P42/nmc*	$a = 3.7205$ $c = 5.2555$	6.7 Ce(1 0 1)	41.0
ZrO_2	Monoclinic *P21/c*	$a = 5.3129$ $b = 5.2125$ $c = 5.1471$ $\beta = 99.218$	23.4 Zr(−1 1 1)	4.5
	Tetragonal *P42/nmc*	$a = 3.5984$ $c = 5.1520$	19.0 Zr(1 0 1)	

[a] Determined by XRD.
[b] Determined by N_2-BET.

monoclinic (JCPDS: 00-037-1484) and tetragonal one (JCPDS: 00-050-1089). No phase segregation for $Ce_{1-x}Zr_xO_2$ into a CeO_2-rich and ZrO_2-rich mixture is detected suggesting that ZrO_2 is incorporated into the CeO_2 lattice to form a solid solution. According to literature [48,49], for the Ce-Zr binary oxides the existence of monoclinic, tetragonal and cubic structures and several stable or metastable phases with tetragonal symmetry was observed. In the case of the investigated Ce-Zr mixed oxides, at high CeO_2 concentration (75 mol%), the cubic phase is favoured, whereas both for intermediate (50 mol%) and ZrO_2-rich (75 mol%) composition, tetragonal was preferential. Simultaneously, a slight shift of the main diffraction peaks to higher 2Θ values, with an increasing amount of ZrO_2 incorporated into CeO_2 is noticed. This observation indicates that the substitution of Ce^{4+} cation (Ce^{4+} cation radius 0.97 Å) with the smaller Zr^{4+} cation (Zr^{+4} cation radius 0.84 Å) causes lowering of symmetry and a decrease in unit cell parameters, as presented in Table 1.

Moreover, comparing to the XRD pattern of CeO_2, the main diffraction peaks observed for the $Ce_{1-x}Zr_xO_2$ solid solutions become broader. This broadening could be ascribed to the distortion of the cubic phase of fluorite structure due to the incorporation of ZrO_2, resulting in the formation of smaller crystallites (Table 1). It could be seen that ZrO_2 incorporation into CeO_2 significantly decreases the average crystallites size of mixed oxides, with the minimum obtained for $Ce_{0.5}Zr_{0.5}O_2$. Simultaneously, at this composition the phase transition from cubic to tetragonal one was also observed, as previously proposed by Yashima et al. [50].

3.1.2. Reducibility characterization

CO is rather rarely used as a reducing agent during TPR studies comparing to H_2. However, the study of materials for CO-involved reactions by TPR-CO is important. The TPR-CO profiles of CeO_2, ZrO_2 and Ce/Zr mixed oxides are presented in Fig. 3.

Reduction of CeO_2 by CO occurs in two stages with the maxima at 430 °C which can be ascribed to the reduction of the most easily reducible surface capping oxygen, and at 840 °C reflecting bulk reduction of CeO_2 and the creation of lower cerium oxides. Beside the low-temperature peak, a characteristic shoulder at ca. 380 °C is observed. It could be related to the possibility of the formation of intermediate phases as the origin of the low-temperature peak of CeO_2 reduction, as previously proposed by Shyu et al. [51]. ZrO_2 incorporation into CeO_2 gives the material in which reducibility features like relative intensity and the position of peaks are different: the peak present at 430 °C for CeO_2 becomes larger and, on the other hand, that at 840 °C becomes smaller, with the increasing ZrO_2 content. One can observe a slight shift of the maximum of the low-temperature peak towards higher temperature with the decrease in Ce/Zr molar ratio. This special behaviour could be related to the phase distortion, which would alternatively shorten or lengthen the metal–oxygen bonds. Furthermore, the lengthening of the metal–oxygen bond would result in a lower barrier of energy for the oxygen migration in the bulk. Both for CeO_2 and Ce-Zr mixed oxides, besides the low-temperature reduction peak a characteristic shoulder in the temperature range 310–400 °C, depending on Ce/Zr molar ratio is observed. It suggests the existence of at least two types of Ce^{4+} located at different chemical environment, assigned to the reduction of surface or subsurface Ce^{4+}. ZrO_2 is mostly considered to be a non-reducible oxide. However, some authors [52] reported negligible hydrogen consumption during ZrO_2 reduction. The results of our study confirm some reduction of zirconia at a higher temperature starting from 670 °C with the maximum at ca. 850 °C. It must be noted that ZrO_2 shows higher resistance to the reduction by CO, comparing to the other oxides studied in this work.

According to literature [53], in the case of solid solution the promotion of the reduction is attributed to the enhanced oxygen mobility compared to pure oxide. However, the degree of reduction can be a parameter which is better related to the amount of oxygen thermodynamically available at a given temperature. The reduction degrees of the investigated samples by CO were calculated according to the following reduction

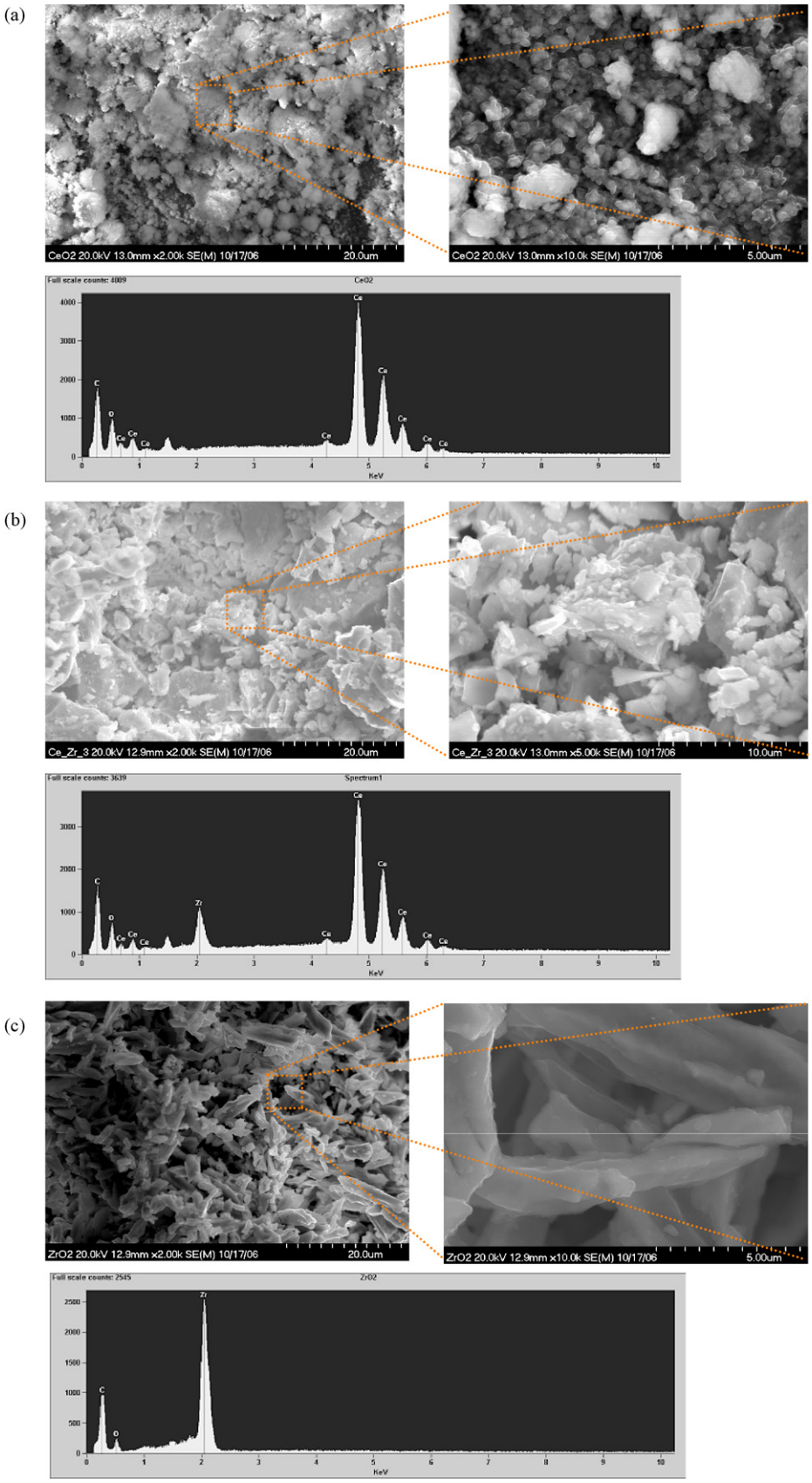

Fig. 1. The secondary electron (SE) photomicrographs and the characteristic X-ray spectra of: (a) CeO_2; (b) $Ce_{0.75}Zr_{0.25}O_2$; (c) ZrO_2.

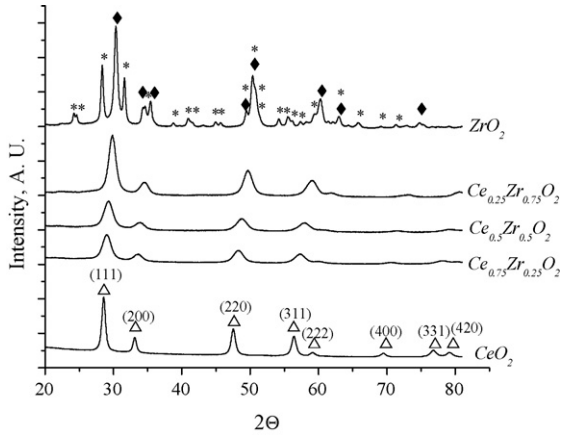

Fig. 2. X-ray diffraction patterns of $Ce_{1-x}Zr_xO_2$ ($x = 0$, 0.25, 0.5, 0.75, 1) oxides: (△) fluorite-type structure (cubic) of CeO_2; (◆) tetragonal-type structure of ZrO_2; (*) monoclinic-type structure of ZrO_2.

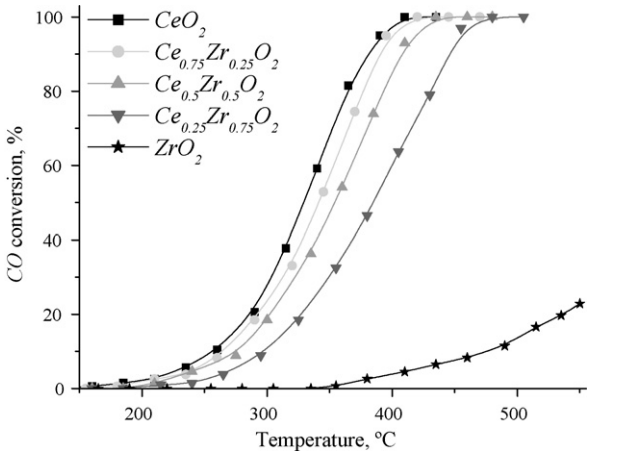

Fig. 4. The activity of $Ce_{1-x}Zr_xO_2$ oxides ($x = 0$, 0.25, 0.5, 0.75, 1) in CO oxidation ($CO:O_2:He = 1.7:3.4:94.9$ vol.%; W/F = 0.12 g s cm^{-3}).

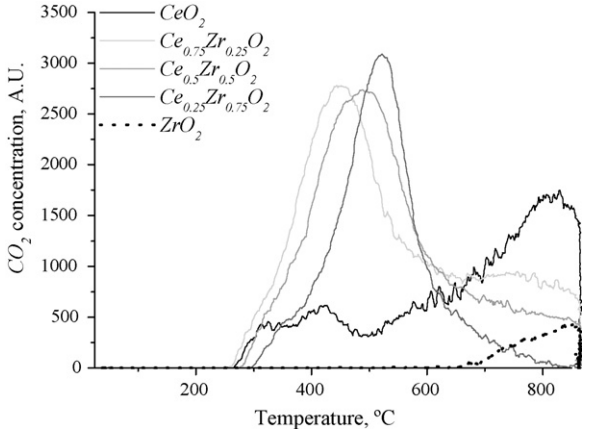

Fig. 3. TPR-CO profiles of $Ce_{1-x}Zr_xO_2$ ($x = 0$, 0.25, 0.5, 0.75, 1) oxides.

processes:

$$CeO_2 + \delta CO \rightarrow CeO_{2-\delta} + \delta CO_2 \quad (2)$$

$$Ce_xZr_{1-x}O_2 + \delta CO \rightarrow Ce_xZr_{1-x}O_{2-\delta} + \delta CO_2 \quad (3)$$

In the case of the mixed oxides the amount of CO_2 formed due to the oxides reduction is higher than for pure CeO_2 and particularly for pure ZrO_2 (Table 2).

Reduction degrees of the investigated oxides were calculated based on the total quantity of CO_2 formed during the reduction, determined on the basis of their reduction profiles (Fig. 3). As it could be seen, the chemical composition of Ce-Zr oxides influences reducibility of Ce^{4+} sites. The reduction degree strongly increases as the zirconium content increases, with the maximum obtained for Ce/Zr molar ratio ≤ 1. Furthermore, these oxides are characterized by tetragonal crystalline phase. On the other hand, the presence of the cubic crystalline phase in the mixed oxides promotes the Ce^{4+} reduction at a lower temperature. As it could be seen, the structural modifications have some relevance to the quantity of oxygen available at given temperatures, which is in fact dependent on the sample composition.

3.1.3. CO oxidation

In order to differentiate the specific contribution of the oxide supports and Au nanoparticles to the CO oxidation, a catalytic investigation of metal-free oxides was performed. Fig. 4 shows a representative series of curves illustrating the effect of temperature on CO conversion over $Ce_{1-x}Zr_xO_2$ oxides in CO oxidation under stationary conditions. The temperature at which the CO conversion reached 10 and 50% (T_{10}, T_{50}) is taken as a measure of catalytic activity.

Typical smooth light-off behaviour is observed and CO conversion increases slightly with temperature. In the case of all investigated oxides, no CO conversion at temperatures below 200 °C was observed. According to the TPR-CO results, in that temperature range their reduction does not occur. The activity towards CO elimination increases at ca. 250–280 °C, depending on a sample composition. Also, at this temperature the reduction of oxides by CO starts. No marked differences in

Table 2
Summary of TPR-CO results of $Ce_{1-x}Zr_xO_2$ oxides

Oxide composition	Temperature (°C)		Total CO_2 formation (mmol g^{-1})	The reduction degree (%)	Estimated oxide composition after reduction
	Peak I	Peak II			
CeO_2	430	840	0.99	34.1	$CeO_{1.83}$
$Ce_{0.75}Zr_{0.25}O_2$	460	760	1.37	58.4	$Ce_{0.75}Zr_{0.25}O_{1.78}$
$Ce_{0.5}Zr_{0.5}O_2$	500	760	1.33	78.6	$Ce_{0.5}Zr_{0.5}O_{1.80}$
$Ce_{0.25}Zr_{0.75}O_2$	530	–	0.87	94.3	$Ce_{0.25}Zr_{0.75}O_{1.88}$
ZrO_2	850	–	0.2	–	–

the activity of CeO_2, $Ce_{0.75}Zr_{0.25}O_2$ and $Ce_{0.5}Zr_{0.5}O_2$ up to 300 °C are observed. Only at higher temperatures of the reaction, more significant differences in CO conversion depending on Ce/Zr molar ratio are noticed. The activity of mixed oxides in CO oxidation was found to be dependent on Ce/Zr molar ratio. The CO conversion increases with an increasing cerium content with maximum activity obtained for $Ce_{0.75}Zr_{0.25}O_2$ (Ce/Zr molar ratio = 3), with the total CO conversion at 420 °C. However, this last activity was comparable to that of CeO_2. One can suggest that cerium is responsible for the activity of mixed oxides in CO oxidation under stationary conditions, as reported before by González-Velasco et al. [54] and Boaro et al. [55]. Only the activity of ZrO_2 in the investigated temperature range was very low (25% CO conversion at 550 °C).

Summarizing, the activity of the investigated oxides increases in the following order: $ZrO_2 < Ce_{0.25}Zr_{0.75}O_2 < Ce_{0.5}Zr_{0.5}O_2 < Ce_{0.75}Zr_{0.25}O_2 < CeO_2$. Taking into consideration the obtained TPR-CO results, one can say that the sequence of decreasing temperature of the maximum reduction peak clearly follows the sequence of increasing activity of the oxides. The observed correlations indicate that ceria which is reducible at the lowest temperatures appears to be responsible for the activity of those oxides in CO oxidation. Moreover, both CeO_2 and $Ce_{0.75}Zr_{0.25}O_2$ are characterized by the cubic crystalline phase and the highest activity in CO oxidation. Thus, it can be suggested that the presence of cubic phase in Ce-Zr solid solution improves its catalytic activity in CO oxidation.

CO oxidation over ceria-containing oxides may follow different mechanisms depending on the experimental conditions and catalysts composition. In order to clarify the role of the oxides used as supports for Au nanoparticles, particularly the possibility of oxygen supply for the reaction, the activity tests using different feedstream composition were also performed. As the first step, the effect of the gas mixtures composition (CO/O_2 ratio) on T_{10} and T_{50} over the metal-free oxides was investigated. The results are presented in Fig. 5.

No marked differences are observed in the temperature ranges characteristic of CO oxidation over $Ce_{1-x}Zr_xO_2$ oxides depending on the investigated CO/O_2 ratios. Only over ZrO_2, 50% CO conversion in the temperature range 25–550 °C cannot be obtained. The activity of mixed oxides was found to be dependent on Ce/Zr molar ratio. $Ce_{0.75}Zr_{0.25}O_2$ shows the lowest temperature of 10 and 50% CO conversion in both stoichiometric and lean in O_2 gas mixture. According to the TPR-CO results, the highest quantity of oxygen that can be involved in the reaction is available at the same temperatures at which CO oxidation occurs. Therefore, the reaction involves an alternate reduction and oxidation of Ce-containing oxide with the formation of surface oxygen vacancies and their successive replenishment by gas-phase oxygen. If a sufficient quantity of oxygen is present in the gas phase (stoichiometric and rich in O_2 gas mixture), it reoxidizes the support and an increase in activity is observed. If lean in O_2 gas mixture was used, the activity would reach the maximum (50% CO conversion) in the temperature range 350–400 °C, depending on the sample composition. At this temperature range, the CO oxidation by bulk oxygen is not possible (see Fig. 3). However, an increase in temperature of the reaction does not cause an increase in CO conversion. It suggests that mostly the surface sites are involved in the reaction. On the other hand, considering TPR-CO experiments as CO oxidation reaction performed without O_2 present in the gas phase, particularly for CeO_2 it is possible to see that under totally anaerobic conditions the activity seems to be dependent on the ability of the oxide to release first the surface and then bulk oxygen. Under these conditions CO oxidation is positively dependent on the degree of reduction of the oxides.

3.2. The characterization of ceria, zirconia and ceria-zirconia supported gold catalysts

3.2.1. Textural and morphological characterization

Table 3 presents the specific surface area, the real Au loading and the Au particle size of $Au/Ce_{1-x}Zr_xO_2$ catalysts.

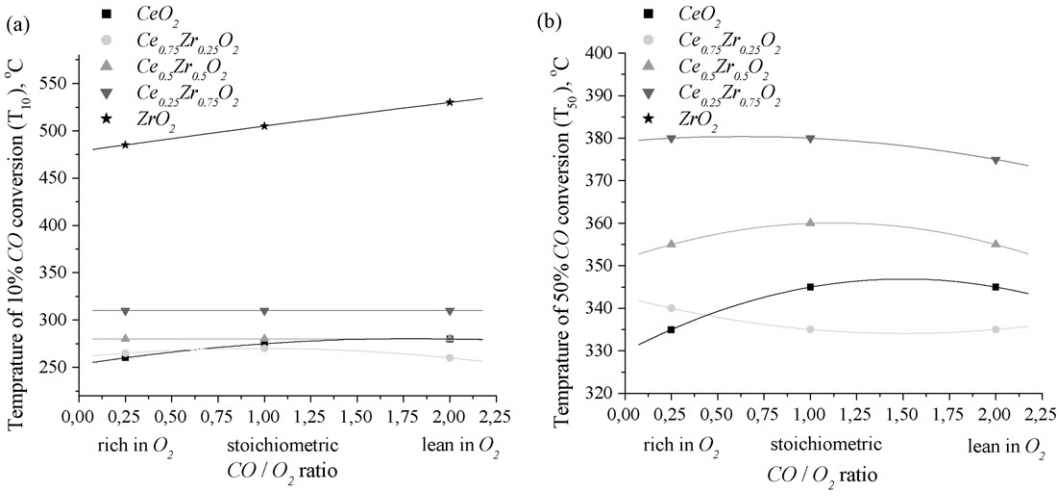

Fig. 5. T_{10} (a) and T_{50} (b) vs. CO/O_2 ratio over $Ce_{1-x}Zr_xO_2$ oxides (rich in O_2, $CO:O_2$:He = 1.7:3.4:94.9 vol.%; W/F = 0.12 g s cm^{-3}; stoichiometric, $CO:O_2$:He = 3.4:1.7:94.9 vol.%; W/F = 0.12 g s cm^{-3}; lean in O_2, $CO:O_2$:He = 4.1:1.0:94.9 vol.%; W/F = 0.12 g s cm^{-3}).

Table 3
The specific surface area, the real Au loading and the Au particle size of $Au/Ce_{1-x}Zr_xO_2$ catalysts

Catalyst denotation (the first number corresponds to the nominal wt.% content of Au)	Surface area[a] ($m^2\ g^{-1}$)	Real gold loading[b] (wt.%)	Au particle size[c] (nm)	D_{Au}[d] (nm)
$2Au/CeO_2$	51.5	1.79	n.d.	4.0
$2Au/Ce_{0.75}Zr_{0.25}O_2$	49.5	1.68	n.d.	3.9
$2Au/Ce_{0.5}Zr_{0.5}O_2$	45	1.74	n.d.	–
$2Au/Ce_{0.25}Zr_{0.75}O_2$	40.7	1.71	n.d.	–
$2Au/ZrO_2$	3.8	1.45	n.d.	5.6
$5Au/CeO_2$	49.7	3.49	n.d.	4.9
$5Au/Ce_{0.75}Zr_{0.25}O_2$	48	3.31	n.d.	4.4
$5Au/ZrO_2$	3.6	1.38	n.d.	5.8

n.d.: Not detectable by XRD.
[a] Determined by N_2-BET.
[b] Determined by AAS (samples washed with ammonia).
[c] Determined by XRD.
[d] Determined by HRTEM, D_{Au}, average diameter of Au particles.

The results of BET measurements indicate that the loading of Au by the DAE method slightly decreases the specific surface area of a given support. However, it diminishes with a further increase in the Au loading. Similarly to the oxide supports, Au/CeO_2 and $Au/Ce_{0.75}Zr_{0.25}O_2$ show the highest surface area and the lowest one is observed for Au/ZrO_2. The similar correlation was found for the catalysts containing the higher amount of Au. It should be noted that the effect of Au on the supports specific surface area is less significant when it is deposited on mixed oxide, than on the monocomponent ones. This could be related to the Zr^{+4} incorporation into the CeO_2 lattice which significantly improves its specific stability.

The nominal gold loading was either 2 or 5 wt.%. A washing of the catalysts with ammonia prior to the drying process causes the loss of ca. 10–15% of gold, compared to those prepared without the washing stage (ca. 2 wt.%). It is not surprising since it is known that during the ammonia washing Cl^- ligands are replaced with OH groups in the exchanged Au species [56]. In addition, gold complexes simply adsorbed on the support due to the lack of OH groups are removed from the surface by washing procedures. However, the quantity of residual chlorine found for Au catalysts washed with ammonia is lower than 200 ppm, as previously reported by the authors for Au/Mg_4Al_2 [25] and later confirmed by Ivanova et al. for Au/CeO_2 [57]. Only when ZrO_2 was used as a support, around 20% loss of Au during its preparation was observed. Considering that the value of the isoelectric point of all supports is similar (ZrO_2, IEP 6.7; CeO_2, IEP 6.75) and higher than the pH of gold precursor $HAuCl_4$ in the concentration of 2.25×10^{-4} M (pH 3.5), similar conditions of preparation can be expected (anions adsorption) [58]. Moreover, zirconia exhibits strong Lewis-type acidity, which was also found to be beneficial to an anionic exchange [59]. Those findings suggest that the observed loss of Au during Au/ZrO_2 preparation could be related to the low specific surface area of zirconia, comparing to the rest of the used oxides.

For higher loaded samples the quantity of Au deposited on all supports is lower than the nominal 5 wt.% (Table 3). Considering that the anionic exchange at the surface depends on the accessible adsorption sites, the influence of the specific surface area of the support on its adsorption ability seems to be significant. If the specific surface area of the support is too small, the number of the adsorption sites is insufficient and Au remains in the solution, resulting in the loss of gold during the catalyst preparation [60]. The maximum Au content deposited over the studied CeO_2, $Ce_{0.75}Zr_{0.25}O_2$ and ZrO_2 was 3.86, 3.65 and 1.85 wt.%, respectively. However, washing of the catalysts with ammonia prior to the drying process causes also the loss of Au (Table 3).

BSE photomicrographs, EDS maps and characteristic X-ray spectra of 2 wt.% Au catalysts supported on CeO_2, $Ce_{0.75}Zr_{0.25}O_2$ and ZrO_2 are given in Fig. 6.

The impregnation of CeO_2 with chloroauric acid ($HAuCl_4$) does not lead to the aggregation of spherical grains of the oxide. Also, no agglomeration of the regular and plated shaped particles of $Ce_{0.75}Zr_{0.25}O_2$ and angular particles of ZrO_2 is observed [61]. However, $2Au/CeO_2$ catalyst washed with ammonia presents the smaller spherical grain size of the oxide. On the other hand, such effect is not observed neither for regular and plated shaped particles of $Ce_{0.75}Zr_{0.25}O_2$ nor angular particles of ZrO_2. The homogenous distribution of Au on the supports surface is observed. The elemental content of all powders appears to be relatively uniform. As confirmed by the BSE photomicrographs and EDS maps, neither the microareas corresponding to the higher Au concentration nor Au clusters were found. The increase in the Au loading does not greatly enhance a homogenous distribution of Au on the support (Fig. 6d).

X-ray diffractograms of CeO_2 supported catalysts with different Au loading are presented in Fig. 7.

A single cubic phase, fluorite-type structure of ceria is observed in Au/CeO_2 catalysts. However, a shift of the four main diffraction peaks corresponding to the (1 0 1) (1 1 0) (2 0 0) (2 1 1) reflections typical of a face-centred cubic (fcc) cell towards lower 2θ angles is observed. The characteristic shift is more significant for the catalyst containing higher Au loading. The observed effect could be related to the lattice expansion due to the formation of Ce^{3+} cations, having a bigger radius than Ce^{4+} (1.14 Å vs. 0.97 Å) [62], suggesting the autoreduction of the catalysts surface during the calcination process. The crystal size of CeO_2 in $2Au/CeO_2$ calculated from

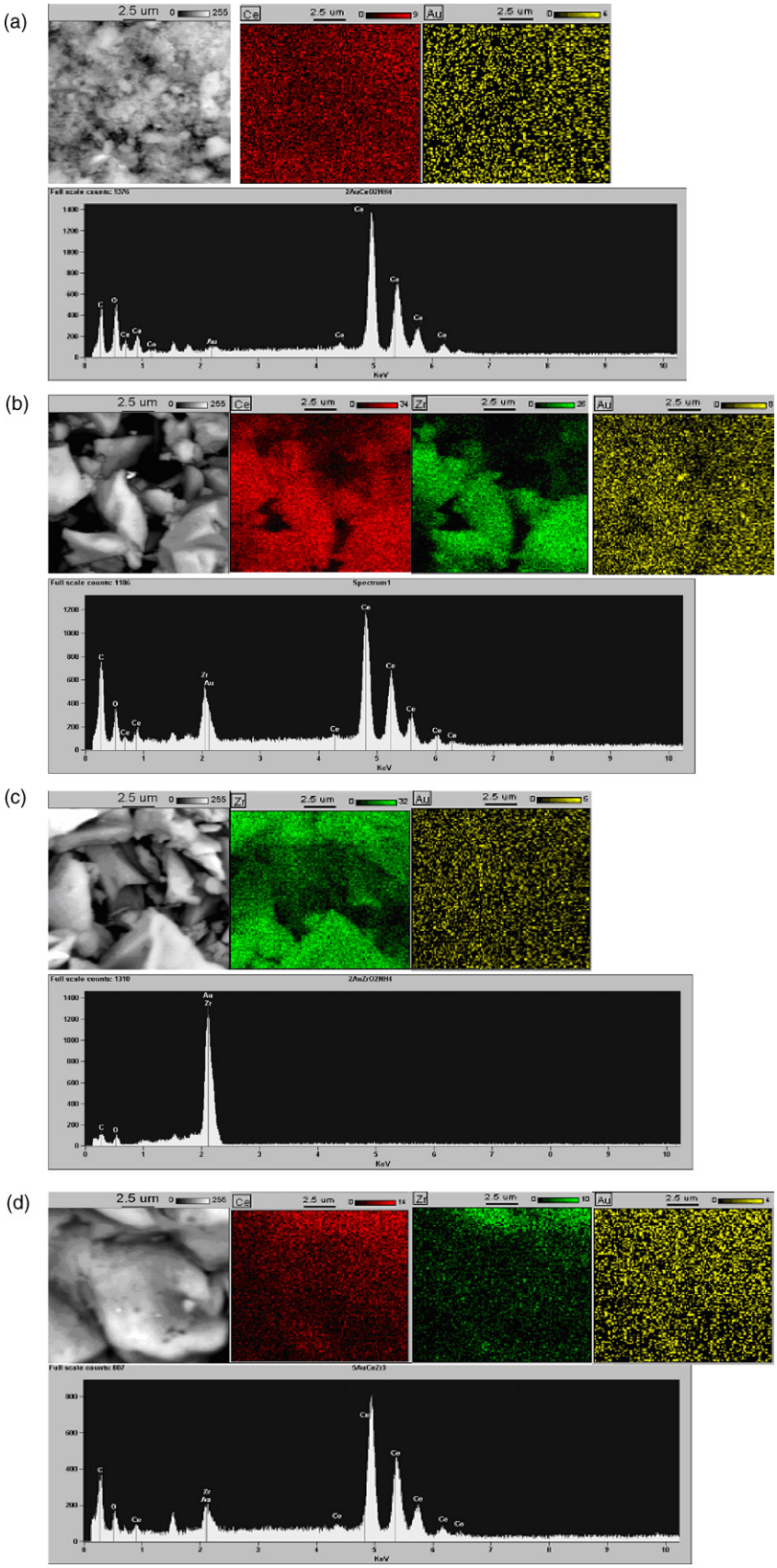

Fig. 6. The back-scattered electron (BSE) photomicrographs, EDS maps and characteristic X-ray spectra of: (a) 2Au/CeO_2; (b) 2Au/$Ce_{0.75}Zr_{0.25}O_2$; (c) 2Au/ZrO_2; (d) 5Au/$Ce_{0.75}Zr_{0.25}O_2$ catalysts.

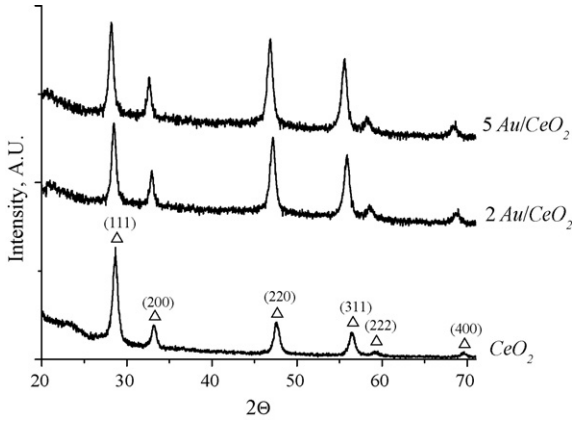

Fig. 7. X-ray diffraction patterns of CeO_2 and Au/CeO_2 catalysts with different Au loading: (△) fluorite-type structure (cubic) of CeO_2.

cerianite (1 1 1) plane is 6.4 nm, twice lower than that estimated for the catalyst prepared excluding this preparation stage. In the case of $2Au/CeO_2$-ZrO_2, at high CeO_2 concentration (75 mol%) in the support, the cubic phase is favoured, whereas both for intermediate (50 mol%) and ZrO_2-rich (75 mol%) composition, tetragonal one was preferential (patterns not presented here). The crystallite size of the support calculated using (1 1 1) diffraction peak in the case of $Ce_{0.75}Zr_{0.25}O_2$ is 7.2 and using (1 0 1) plane in the case of $Ce_{0.5}Zr_{0.5}O_2$ and $Ce_{0.25}Zr_{0.75}O_2$ is 6.7 and 7, respectively. The crystal size of ZrO_2 in $2Au/ZrO_2$ calculated based on the baddeleyite (−1 1 1) and tetragonal (1 0 1) planes is 27.8 nm and 18.8 nm, respectively. In the case of all studied catalysts no clear Au reflections are observed. It suggests that either well-dispersed small Au particles are present on the support surface or the Au loading is too low to be detected. Also, the XRD pattern of Au/CeO_2 catalyst containing 3.49 wt.% of Au does not contain characteristic Au reflections, which suggests the presence of well-dispersed small Au particles on the support surface (Table 3).

HRTEM technique was used in order to determine an average Au particle size and to define their distribution more accurate (Table 3). For the catalysts containing 2 wt.% of Au, the majority of the Au particles supported on CeO_2 and $Ce_{0.75}Zr_{0.25}O_2$ are in the range of 1–5 nm, with the mean particle diameter of approximately 4 nm. For ZrO_2 supported catalyst, the major part of gold particles is in the range of 1–7 nm, with the mean particle diameter 5.6 nm.

The average Au particle size for the catalysts containing higher Au loading is presented in Table 3. The majority of the Au particles supported on CeO_2 and $Ce_{0.75}Zr_{0.25}O_2$ are also in the range of 1–7 nm, whereas for Au/ZrO_2 catalyst 1–9 nm.

3.2.2. Reducibility characterization

The reducibility of the investigated catalysts as potential materials for CO-involved reactions, was also studied by TPR-CO. Fig. 8 presents the effect of well-dispersed Au nanoparticles on the reducibility of $Ce_{1-x}Zr_xO_2$ oxides.

In the temperature range 25–500 °C two overlapping peaks are registered in the TPR-CO profiles of CeO_2, $Ce_{0.75}Zr_{0.25}O_2$ and $Ce_{0.5}Zr_{0.5}O_2$ based Au catalysts. Also, in the case of the oxide supports, beside the reduction peak a characteristic shoulder was observed at low temperature. This suggests the existence of at least two types of Ce^{4+}, surface and subsurface, located at different chemical environments that in the presence of well-dispersed Au are susceptible to the reduction at lower temperatures. On the other hand, the reduction peaks present at a higher temperature remain almost unchanged. The reduction of $Au/Ce_{0.25}Zr_{0.75}O_2$ occurs in one stage with the maximum at ca. 380 °C, similarly to the $Ce_{0.25}Zr_{0.75}O_2$ oxide. However, the temperature range at which the catalysts reduction takes place is significantly lower. For the Au/ZrO_2 catalyst, the TPR-CO profile consists of one peak with the maximum at ca. 820 °C.

Summarizing, in the presence of Au, the characteristic reduction peaks of Ce-containing support oxides are shifted towards lower temperatures. One can observe that the most important difference among the analysed samples lies in the temperature at which catalysts reduction starts (Table 4). The lowest temperature is observed for $Ce_{0.75}Zr_{0.25}O_2$ and CeO_2 based Au catalysts. Furthermore, this effect is even more significant for the samples with the higher gold loading (Fig. 8b). It can be seen that the low-temperature reduction peak is slightly shifted to a higher temperature with the increasing gold loading, while the high temperature reduction peak remains unaffected.

As it could be seen, the presence of Au effectively promotes the reduction of supports at low temperature. The promoting

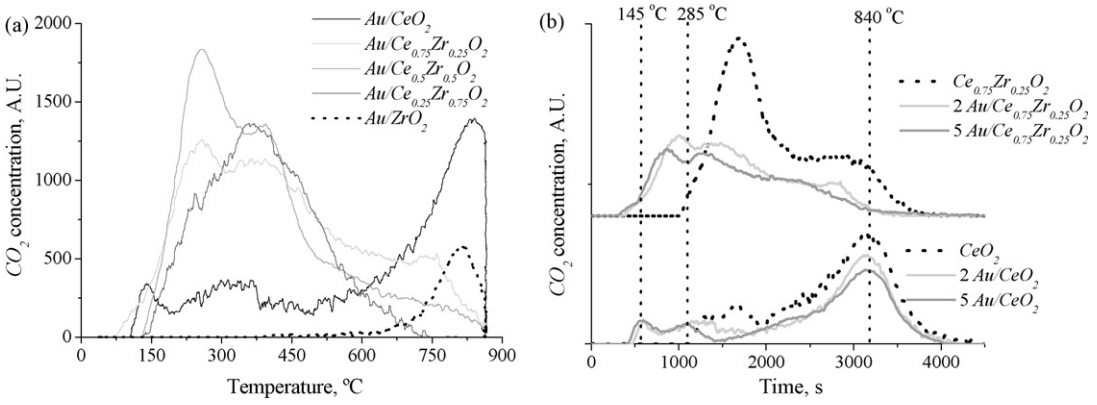

Fig. 8. TPR-CO profiles of: (a) $2Au/Ce_{1-x}Zr_xO_2$; (b) CeO_2 and $Ce_{0.75}Zr_{0.25}O_2$ supported catalysts with various Au loading.

Table 4
Summary of TPR-CO results of $Au/Ce_{1-x}Zr_xO_2$ catalysts

Catalyst denotation (the first number corresponds to the nominal wt.% content of Au)	Temperature (°C)				CO_2 formation (mmol g^{-1})
	T^0 (initial)	Peak I	Peak II	Peak III	
$2Au/CeO_2$	110	150	320	840	0.75
$2Au/Ce_{0.75}Zr_{0.25}O_2$	85	260	380	740	0.90
$2Au/Ce_{0.5}Zr_{0.5}O_2$	135	270	400	720	0.87
$2Au/Ce_{0.25}Zr_{0.75}O_2$	140	380	–	–	0.67
$2Au/ZrO_2$	670	820	–	–	0.14
$5\ Au/CeO_2$	95	145	285	840	0.67
$5\ Au/Ce_{0.75}Zr_{0.25}O_2$	65	220	340	610	0.80
$5\ Au/ZrO_2$	670	820	–	–	0.13

effect of dispersed Au on the reducibility of different metal oxides support has already been observed [63–65]. Moreover, such enhanced reduction behaviour has also been reported for the other noble metals (Pt, Rh, Pd) supported on CeO_2, ZrO_2 and Ce-Zr mixed oxides [66–69]. Comparing with the other noble metals, such behaviour could be related to the adsorption of CO molecules on well-dispersed metallic gold particles and next to the migration by a spillover process from the Au particles on the support surface. That process could be favoured by a high dispersion of gold on the support surface. However, if the catalyst contains only ionic gold, the surface oxygen reducibility could be intensified through the lattice substitution mechanism, as reported by Fu et al. [70]. According to those statements, the Au^+ or Au^{3+} ions would fill the vacant Ce^{4+} sites resulting in the oxygen vacancies formation and the increase in oxygen mobility and reducibility. In this case, the presence of gold causes a decrease in the strength of the surface Ce–O bonds adjacent to gold atoms, thus leading to higher surface lattice oxygen mobility, as proposed by Scirè et al. [71].

The summary of the TPR-CO results including the estimated quantity of CO_2 formed during the catalysts reduction, determined on the basis of their reduction profiles, is given in Table 4.

The amount of CO_2 formed during the reduction of the studied catalysts is lower than that observed for the oxide supports. It should be noticed that in the presence of a higher gold loading this effect is even more significant. Considering that washing of the Au catalysts with ammonia allows removing residual chlorine [25], which is known to inhibit the reducibility of Ce-containing oxides, the catalysts autoreduction during the calcination can occur, as we mentioned above. The autoreduction phenomenon can be also the reason for the change in the catalysts colour during drying and calcination processes from yellow to dark grey and from dark grey to graphite, respectively. It can also explain the characteristic shift of main diffraction peaks of CeO_2 in the XRD pattern of ammonia washed catalysts (Fig. 7).

3.2.3. CO oxidation

Fig. 9 presents a representative series of curves showing the effect of temperature on the CO conversion over $Au/Ce_{1-x}Zr_xO_2$ catalysts under stationary conditions. The temperature at which the CO conversion reached 10 and 50% (T_{10}, T_{50}) is taken as a measure of catalytic activity.

The typical smooth light-off behaviour is observed and CO conversion increases with the temperature. The highest activity (100% CO conversion at 68 °C) is observed over the $2Au/Ce_{0.75}Zr_{0.25}O_2$ catalyst. Total CO conversion below 125 °C is possible only in the case of Ce-containing based Au catalysts. $2Au/ZrO_2$ shows much lower activity (total CO conversion is noticed at 300 °C). The effect of gold loading on the catalytic activity of some oxides is presented in Fig. 9b. As it can be seen, samples with the higher Au content exhibit higher CO conversion with the maximum obtained for $5Au/Ce_{0.75}Zr_{0.25}O_2$ (71% CO conversion at 25 °C).

The comparable Au content and its dispersion on CeO_2 and Ce-Zr mixed oxides were confirmed by AAS and TEM techniques. However, the difference in their activity in CO

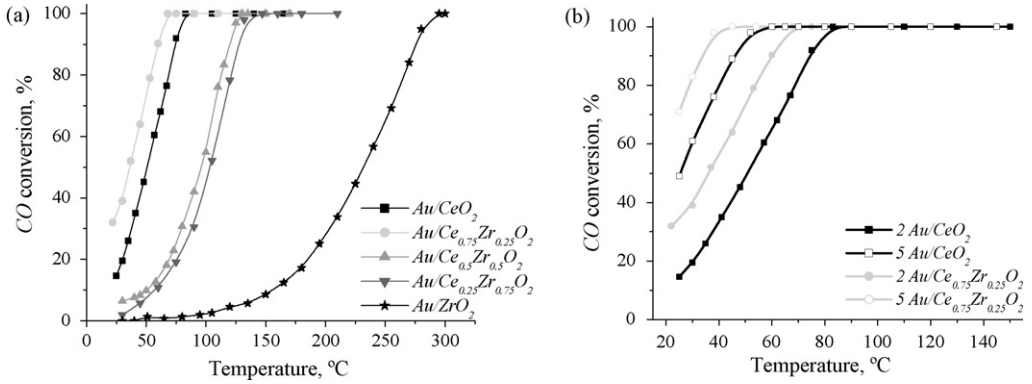

Fig. 9. The activity of: (a) $2Au/Ce_{1-x}Zr_xO_2$ catalysts; (b) CeO_2 and $Ce_{0.75}Zr_{0.25}O_2$ based catalysts with various Au loading in CO oxidation ($CO:O_2$:-He = 1.7:3.4:94.9 vol.%; W/F = 0.12 g s cm^{-3}).

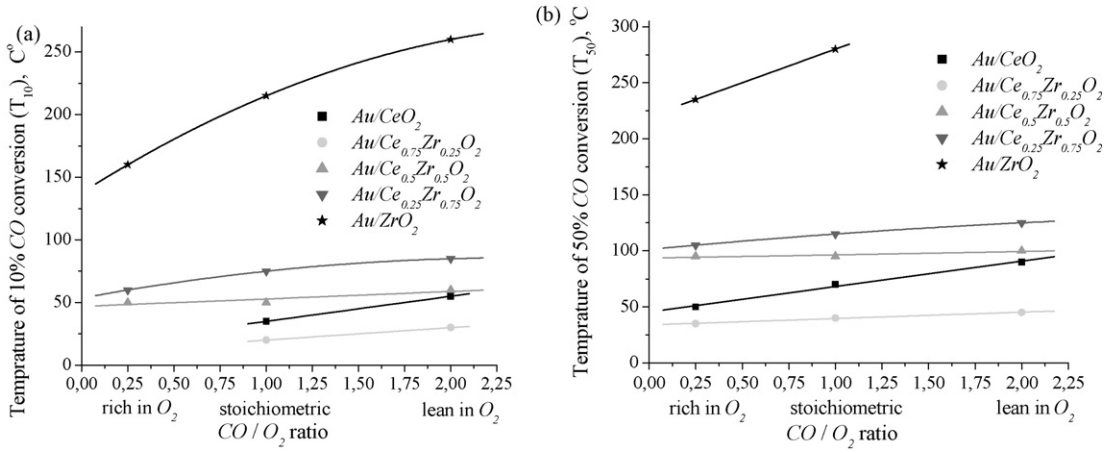

Fig. 10. T_{10} (a) and T_{50} (b) vs. CO/O_2 ratio over $2Au/Ce_{1-x}Zr_xO_2$ catalysts (rich in O_2, CO:O_2:He = 1.7:3.4:94.9 vol.%; W/F = 0.12 g s cm^{-3}; stoichiometric, CO:O_2:He = 3.4:1.7:94.9 vol.%; W/F = 0.12 g s cm^{-3}; lean in O_2, CO:O_2:He = 4.1:1.0:94.9 vol.%; W/F = 0.12 g s cm^{-3}).

oxidation is very well marked. The activity of the studied catalysts was found to be dependent on Ce/Zr molar ratio in the oxide used as a support for Au, increasing in the following order: $Au/ZrO_2 < Au/Ce_{0.25}Zr_{0.75}O_2 \approx Au/Ce_{0.5}Zr_{0.5}O_2 < Au/CeO_2 < Au/Ce_{0.75}Zr_{0.25}O_2$. According to the TPR-CO studies, the presence of highly dispersed Au nanoparticles effectively promotes the reduction of the catalysts surface at a low temperature, especially these based on Ce-rich oxides. This effect is even more pronounced for the catalysts containing a higher amount of well-dispersed Au. One can say that the sequence of the decreasing initial temperature of catalysts reduction clearly follows the sequence of increasing activity. The highest activity in CO oxidation is obtained over the $Au/Ce_{0.75}Zr_{0.25}O_2$ catalyst. Moreover, its reduction starts at the lowest temperature (Table 4). As it can be seen, in the presence of highly dispersed Au nanoparticles, Ce-containing support is susceptible to the reduction at a lower temperature and appears to be responsible for the activity of studied catalysts. For this reason Au nanoparticles deposited on hardly reducible ZrO_2 present lower activity in CO oxidation. These findings indicate the role of a support in creation of the catalytic performance of supported Au nanoparticles in CO oxidation. It should also be noted that in the case of CeO_2 and Ce-Zr mixed oxide supports no CO conversion at temperatures below 200 °C was observed (Fig. 4). Obviously, the presence of well-dispersed Au greatly improves their catalytic performance. This can be attributed to the synergetic effect between the support and gold particles at the interface. The CO adsorption on Au^{3+}, Au^{+}, and Au^{0} species was observed in the case of Au/CeO_2 catalyst by Guzman et al. [72]. The presence of an additional band assigned to Ce^{4+}-CO was also found, confirming CO adsorption on CeO_2. Moreover, under totally anaerobic conditions, CO_2 formation was observed indicating the ability of CeO_2 to supply reactive oxygen to Au active species for oxidation of CO. This supports the idea of CeO_2 acting as an oxygen buffer by releasing–uptaking oxygen through the redox processes involving Ce^{4+}/Ce^{3+} redox couple [62].

Fig. 10 presents the temperatures at which the CO conversion over $2Au/Ce_{1-x}Zr_xO_2$ catalysts reached 10 and 50% (T_{10}, T_{50}) as a function of the gas mixtures composition (CO/O_2 ratio).

No marked differences in the temperature at which CO oxidation occurs depending on the investigated CO/O_2 ratios over Ce-Zr mixed oxides supported Au catalysts are observed. The ability to preserve high activity in stoichiometric and lean in O_2 gas mixtures suggests participation of the support in the

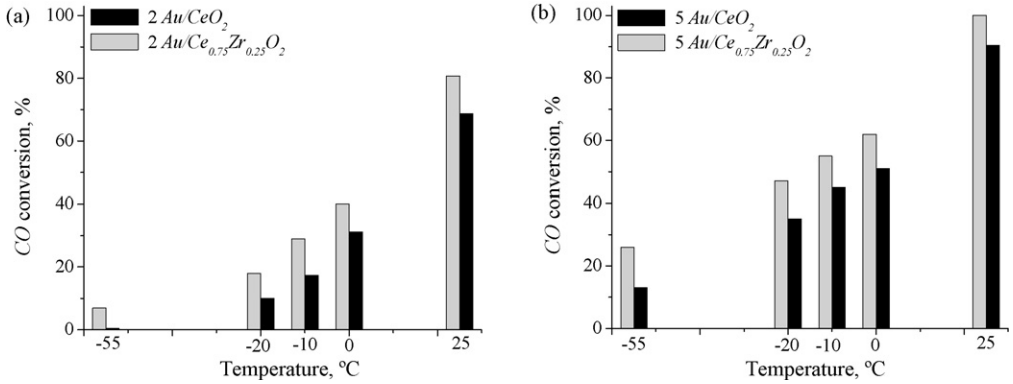

Fig. 11. The activity of Au catalysts supported on CeO_2 and $Ce_{0.75}Zr_{0.25}O_2$ in a CO/air gas mixture, containing (a) 2 wt.% and (b) 5 wt.% of Au (CO:air = 0.24:99.76 vol.%; W/F = 0.12 g s cm^{-3}).

Table 5
Comparison of activity in CO oxidation over CeO_2, ZrO_2 and CeO_2-ZrO_2 supported Au catalysts

Oxide support	Au loading (wt.%)	Preparation method[a]	Catalyst treatment temperature (°C)	Au particle size[b] (nm)	Catalyst weight (mg)	Reaction conditions	Activity		Reference
							CO conversion[c] (%)	T_{50}[d] (°C)	
CeO_2	2.0	SCS	500	n.r.	800	2300 ppm CO, 7%O_2, He balance, W/F = 0.12 g s cm^{-3}	0	272	[8]
CeO_2	3.0	DP	100	n.d.[e]	50	1%CO, 1%O_2, He balance, 50 cm^3 min^{-1}	100	−13	[10]
CeO_2	3.0	DP	300	15[e]	50	1%CO, 1%O_2, He balance, 50 cm^3 min^{-1}	20	47	[10]
CeO_2	3.0	SMAD	25	n.d.[e]	50	1%CO, 1%O_2, He balance, 50 cm^3 min^{-1}	6	97	[10]
CeO_2	2.0	CB	400	8[e]	20	CO/O_2/He = 2/2/96 molar ratio, 50 cm^3 min^{-1}	0	170	[11]
CeO_2	3.0	CB	400	9[e]	20	CO/O_2/He = 2/2/96 molar ratio, 50 cm^3 min^{-1}	0	150	[11]
CeO_2	2.0	DP	110	n.r.	50	3.6%CO, 21%O_2, Ar balance, 1000 cm^3 min^{-1}	90	n.r.	[6]
CeO_2	2.77	DP	120	20–30	150	1%CO, 19%O_2, N_2 balance, 100 cm^3 min^{-1}	80	n.r.	[14]
CeO_2	1.0	DP	180	2–5	60	1%CO, air balance, 50 cm^3 min^{-1}	75	n.r.	[15]
ZrO_2	1.7	SCGC	400	1.9	200	0.25%CO, 0.25%O_2, N_2 balance, GHSV = 12,000 h^{-1}	13	70	[73]
ZrO_2	2.6	DP	200	2	46	1%CO, air balance, 250 cm^3 min^{-1}	n.r.	−18	[17]
ZrO_2	2.6	DP	300	4–8	46	1%CO, air balance, 250 cm^3 min^{-1}	n.r.	50	[17]
ZrO_2	3.0	DP	400	4.1	250	0.18%CO, air balance, 73 cm^3 min^{-1}	65	5	[16]
ZrO_2	0.71	DP	400	4.7	100	1%CO, air balance, 20,400 cm^3 h^{-1} g_{cat}^{-1}	n.r.	80	[12]
ZrO_2	2.0	SCS	500	5–25	800	2.3%CO, 7%O_2, He balance, W/F = 0.12 g s cm^{-3}	0	242	[8]
$Ce_{0.8}Zr_{0.2}O_2$	2.0	DP	300	n.r.	50	0.5 cm^3 min^{-1} CO, 33.3 cm^3 min^{-1} air	0	100	[36]
CeO_2	1.79	DAE	300	4	100	1.6%CO, 3.3%O_2, He balance, 50 cm^3 min^{-1}	15	50	[f]
ZrO_2	1.45	DAE	300	5.6	100	1.6%CO, 3.3%O_2, He balance, 50 cm^3 min^{-1}	0	230	[f]
$Ce_{0.75}Zr_{0.25}O_2$	1.68	DAE	300	3.9	100	1.6%CO, 3.3%O_2, He balance, 50 cm^3 min^{-1}	35	35	[f]

n.d.: Not detectable by XRD; n.r.: not reported.
[a] *Abbreviations*: SCS, combustion synthesis; DP, deposition–precipitation; SMAD, solvated metal atom dispersion; CB, combustion; SCGC, Size controlled gold colloids; DAE, direct anionic exchange.
[b] Determined by TEM.
[c] CO conversion obtained at room temperature.
[d] Temperature at which 50% CO conversion was obtained.
[e] Determined by XRD.
[f] Present work.

CO oxidation not only in providing centres for oxygen activation but also as a buffer in releasing–uptaking oxygen through the redox processes realized by Ce^{4+}/Ce^{3+} redox couple. However, for $2Au/ZrO_2$ catalyst the decrease in O_2 concentration in gas mixture leads to the increase in temperature at which 10 and 50% CO conversion is obtained. It could be related to the lower reducibility of $2Au/ZrO_2$ system and the lack of oxygen storage properties.

The catalytic stability of the most active catalysts was tested at three different temperatures 30, 60 and 90 °C. Both Au/CeO_2 and $Au/Ce_{0.75}Zr_{0.25}O_2$ containing 2 and 5 wt.% of Au show a slight loss of activity (5–8%) during time on stream tests for 5 days performed at 30 °C. However, time on stream studies at 60 and 90 °C shows negligible change in activity. These results show good stability of the studied catalysts.

Considering the potential practical application of the developed Au catalysts their activity tests were also investigated in CO/air gas mixture. CO conversion over the most active catalysts containing 2 and 5 wt.% of Au supported CeO_2 and $Ce_{0.75}Zr_{0.25}O_2$ at different temperatures are shown in Fig. 11.

One can see that the studied catalysts are highly active at room temperature. The samples containing higher Au loading exhibit higher CO conversion, with the maximum obtained for $5Au/Ce_{0.75}Zr_{0.25}O_2$ (100% CO conversion at 25 °C). Moreover, their activity at 0 °C as well as at temperature below 0 °C is also satisfactory. These results suggest that the developed Au catalysts can find practical application, e.g., in closed-cycle CO_2 lasers, purification of breathing air in closed spaces, safety masks and as a material for gas sensors for detection of trace amounts of CO in the air.

The present study has demonstrated the relation between the physico-chemical properties of the supports and the catalytic performance of $Au/Ce_{1-x}Zr_xO_2$ catalysts in CO oxidation. Table 5 presents a brief comparison of some representative activity data obtained in this work with those reported in the literature, taking into consideration different preparation methods, calcination temperature, experimental conditions, gold particle size, etc. The activity of Au/CeO_2 catalysts prepared by both deposition–precipitation and combustion method, calcined respectively at 300 and 400 °C, and tested under similar reaction conditions, is comparable with the data obtained in this paper [10,11]. Moreover, the studied Au/CeO_2 catalyst shows similar activity in CO oxidation in air at room temperature to the ceria supported Au catalysts, as reported in Refs. [14,15]. Recently, Pillai and Deevi [6] have presented exceptionally high activity of Au/CeO_2 synthesized by DP for CO oxidation in air. However, this catalyst was not pretreated in situ before reaction testing. They also reported that the exposure of the catalyst to ambient air over night after its thermal treatment at 100 °C enhances the catalyst activity for the oxidation reaction. It suggests that the observed high activity over Au/CeO_2 could be attributed to the beneficial effect of the adsorption of water molecules from the atmosphere by the catalyst. On the other hand, the temperature of 50% CO conversion reported by Russo et al. [8] was much higher than that obtained by us, even if the O_2/CO ratio used in their catalytic tests (O_2/CO = 30) was much higher than that of our experiments (O_2/CO = 2). On the other hand, the temperature of 50% CO conversion over Au/ZrO_2 catalyst synthesized by so-called SCS method [8] is comparable with the data obtained in our paper. However, the application of dissimilar reaction conditions generates different activities over Au/ZrO_2 catalysts as reported by some authors [16,17,73]. Moreover, the activity in CO oxidation over Au supported on inert oxides depends very critically on the diameter of gold particles, and only extremely small particles (2 nm and below) yield highly active samples [29,74,75]. For those systems oxygen adsorption occurs directly on gold particles, either on defect sites (steps, edges, corners) or it is facilitated by variations in the electronic structure of very small gold particles. It should be noticed that in the case of Au/ZrO_2 catalyst prepared by us, Au particle size was bigger (5.6 nm) than that reported by Baiker and co-workers (1.9 nm) [73]. Also, Wolf and Schüth [17] have presented exceptionally high activity over Au/ZrO_2 synthesized by DP for CO oxidation in air. However, due to the different both reaction conditions and Au loading it is difficult to compare those data with our catalytic results.

From all $Au/Ce_{1-x}Zr_xO_2$ catalysts studied in this paper, the highest activity was observed over the $2Au/Ce_{0.75}Zr_{0.25}O_2$ one. As we mentioned above, only few papers have reported the study of Au supported on ceria-zirconia as catalysts for CO oxidation. Very recently, Wang et al. [36] presented the study over the synthesis, characterization and catalytic activity of $Au/Ce_{0.8}Zr_{0.2}O_2$ systems in oxidation of CO. They reported that Au (2 wt.%)/$Ce_{0.8}Zr_{0.2}O_2$ catalyst prepared by deposition–precipitation method showed the best catalytic performance among all the prepared samples. However, the temperature of 50% CO conversion observed for Au (1.68 wt.%)/$Ce_{0.75}Zr_{0.25}O_2$ catalyst studied in our work is much lower than that of the most active one employed in Ref. [36]. It should be noted (Table 5) that different concentration of CO and O_2 were used in the two studies. This, however, does not pose problems for comparison, since both CO/O_2 molar ratio and gold loading are higher and simultaneously the activity of the catalyst synthesized by Wang and co-workers is lower. The higher activity of our catalyst could be attributed to the preparation procedures of both support and catalyst that influences their physico-chemical properties.

4. Conclusions

The physico-chemical properties and activity of Ce-Zr mixed oxides, CeO_2 and ZrO_2 as supports for Au catalysts in CO oxidation have been studied from the point of view of their contribution to the reaction. An influence of the supports on the catalytic performance of $Au/Ce_{1-x}Zr_xO_2$ catalysts in the reaction of CO oxidation has been investigated. The most significant results can be summarized as follows:

- ZrO_2 incorporation into CeO_2 lattice leads to significant modifications in the redox properties of ceria. The presence of a tetragonal structure in mixed oxides leads to an increase in Ce^{4+} content available for the reduction at lower tempera-

tures. Mixed oxides with Ce/Zr molar ratio ≤ 1 show the highest total reduction degree.

- The results of this study confirm some reduction of zirconia at high temperature. It must be noted that ZrO_2 is mostly considered to be a non-reducible oxide.
- The activity of the investigated oxides in CO oxidation increases in the following order: $ZrO_2 < Ce_{0.25}Zr_{0.75}O_2 < Ce_{0.5}Zr_{0.5}O_2 < Ce_{0.75}Zr_{0.25}O_2 < CeO_2$.
- The activity of mixed oxides in CO oxidation was found to be dependent on Ce/Zr molar ratio and related to their reducibility and/or oxygen mobility.
- The role of a support in the creation of the catalytic performance of supported Au nanoparticles in CO oxidation is significant. Ceria, which is susceptible to reduction at the lowest temperature, in the presence of highly dispersed Au nanoparticles, appears to be responsible for the activity of the studied catalysts.
- CeO_2-ZrO_2 mixed oxides are promising supports for Au nanoparticles in CO oxidation, whose activity was also found to be dependent on Ce/Zr molar ratio.
- For the studied catalysts the sequence of the increasing reducibility clearly follows the sequence of the increasing activity, which suggests that CO oxidation is affected by similar factors influencing the reduction process.
- The ability to preserve high activity in stoichiometric and lean in O_2 gas mixtures suggests the participation of the support in CO oxidation not only in providing centres for oxygen activation but also as a buffer in releasing–uptaking oxygen through redox processes realized by Ce^{4+}/Ce^{3+} redox couple. It can be attributed to the synergetic effect between the support and gold particles at the interface.
- Au/CeO_2 and $Au/Ce_{0.75}Zr_{0.25}O_2$ catalysts show a negligible change in activity during time on stream tests for 5 days.
- Very high activity of Au/CeO_2 and $Au/Ce_{0.75}Zr_{0.25}O_2$ catalysts in a CO/air gas mixture at room temperature and 0 °C as well as at temperature below 0 °C, suggests that developed Au catalysts could find practical application e.g., in closed-cycle CO_2 lasers, purification of breathing air in closed spaces, safety masks and as a material for gas sensors for detection of trace amounts of CO in the air.

Acknowledgments

This research was supported by Grant PBZ-KBN-116/T09/2004 (No. K124/1B/2005).

The authors are grateful to Dr. W. Maniukiewicz for performing XRD measurements and to Dr. Miguel Ángel Gómez García for fruitful discussions.

Izabela Dobrosz-Gómez is a holder of a fellowship of the Mechanism WIDDOK program supported by European Social Fund and Polish State (contract number WIDDOK/SM/2006/7).

References

[1] M. Haruta, T. Kobayashi, H. Sano, N. Yamada, Chem. Lett. 2 (1987) 405–408.
[2] G.J. Hutchings, M.R.H. Siddiqui, A. Burrows, C.J. Kiely, R. Whyman, J. Chem. Soc. Faraday Trans. 93 (1) (1997) 187–188.
[3] G.C. Bond, D.T. Thompson, Cat. Rev. -Sci. Eng. 41 (3–4) (1999) 319–388.
[4] N.A. Hodge, C.J. Kiely, R. Whyman, M.R.H. Siddiqui, G.J. Hutchings, Q.A. Pankhurst, F.E. Wagner, R.R. Rajaram, S.E. Golunski, Catal. Today 72 (2002) 133–144.
[5] G.J. Hutchings, M.S. Hall, A.F. Carley, P. Landon, B.E. Solsona, C.J. Kiely, A. Herzing, M. Makkee, J.A. Moulijn, A. Overweg, J.C. Fierro-Gonzalez, J. Guzman, B.C. Gates, J. Catal. 242 (2006) 71–81.
[6] U.R. Pillai, S. Deevi, Appl. Catal. A: Gen. 299 (2006) 266–273.
[7] S.-Y. Lai, Y. Qiu, S. Wang, J. Catal. 237 (2006) 303–313.
[8] N. Russo, D. Fino, G. Saracco, V. Specchia, Catal. Today 117 (2006) 214–219.
[9] V. Idakiev, T. Tabakova, A. Naydenov, Z.-Y. Yuan, B.-L. Su, Appl. Catal. B: Environ. 63 (2006) 178–186.
[10] M.P. Casaletto, A. Longo, A.M. Venezia, A. Martorana, A. Prestianni, Appl. Catal. A: Gen. 302 (2006) 309–316.
[11] F. Arena, P. Famulari, G. Trunfio, G. Bonura, F. Frusteri, L. Spadaro, Appl. Catal. B: Environ. 66 (2006) 81–91.
[12] X. Zhang, H. Wang, B.-Q. Xu, J. Phys. Chem. B 109 (2005) 9678–9683.
[13] X. Zhang, H. Shi, B.-Q. Xu, Catal. Today 122 (2007) 330–337.
[14] C. Sun, H. Lia, L. Chen, J. Phys. Chem. Solids 68 (2007) 1785–1790.
[15] L.-H. Chang, N. Sasirekha, B. Rajesh, Y.-W. Chen, Sep. Purif. Technol. 58 (2007) 211–218.
[16] P. Konova, A. Naydenov, T. Tabakova, D. Mehandjiev, Catal. Commun. 5 (2004) 537–542.
[17] A. Wolf, F. Schüth, Appl. Catal. A: Gen. 226 (2002) 1–13.
[18] G.J. Hutchings, M. Haruta, Appl. Catal. A: Gen. 291 (2005) 2–5.
[19] G.J. Hutchings, Catal. Today 100 (2005) 55–61.
[20] Q. Fu, S. Kudriavtseva, H. Saltsburg, M. Flytzani-Stephanopoulos, Chem. Eng. J. 93 (1) (2003) 41–53.
[21] W. Deng, J. De Jesus, H. Saltsburg, M. Flytzani-Stephanopoulos, Appl. Catal. A: Gen. 291 (2005) 126–135.
[22] Q. Fu, W. Deng, H. Saltsburg, M. Flytzani-Stephanopoulos, Appl. Catal. B: Environ. 56 (2005) 57–68.
[23] M. Manzoli, F. Boccuzzi, A. Chiorino, F. Vindigni, W. Deng, M. Flytzani-Stephanopoulos, J. Catal. 245 (2007) 308–315.
[24] G.J. Hutchings, A.A. Mirzaei, R.W. Joyner, M.R.H. Siddiqui, S.H. Taylor, Appl. Catal. A: Gen. 166 (1998) 143–152.
[25] I. Dobrosz, K. Jiratova, V. Pitchon, J.M. Rynkowski, J. Mol. Catal. A: Chem. 234 (2005) 187–197.
[26] F. Arena, P. Famulari, N. Interdonato, F. Frusteri, L. Spadaro, Catal. Today 116 (2006) 384–390.
[27] Z. Ma, S.H. Overbury, S. Dai, J. Mol. Catal. A: Chem. 273 (2007) 186–197.
[28] Z. Ma, C. Liang, S.H. Overbury, S. Dai, J. Catal. 252 (2007) 119–126.
[29] M.M. Schubert, S. Hackenberg, A.C. van Veen, M. Muhler, V. Plzak, R.J. Behm, J. Catal. 197 (2001) 113–122.
[30] B. Grzybowska-Świerkosz, Catal. Today 112 (2006) 3–7.
[31] A.S.K. Hashmi, G.J. Hutchings, Angew. Chem. Int. Ed. 45 (2006) 7896–7937.
[32] A. Trovarelli (Ed.), Catalysis by ceria and related materials, ICP, 2002, pp. 15–50.
[33] M. Daturi, C. Binet, J.C. Lavalley, G. Blanchard, Surf. Interface Anal. 30 (2000) 273–277.
[34] M.A. Gómez-García, V. Pitchon, A. Kiennemann, Environ. Int. 31 (2005) 445–467 (and references therein).
[35] I. Dobrosz, M.A. Gómez-García, I. Kocemba, W. Maniukiewicz, J.M. Rynkowski, Pol. J. Environ. Stud. 14 (IV) (2005) 231–234.
[36] S.-P. Wang, T.-Y. Zhang, X.-Y. Wang, S.-M. Zhang, S.-R. Wang, W.-P. Huang, S.-H. Wu, J. Mol. Catal. A: Chem. 272 (2007) 45–52.
[37] P. Haider, A. Baiker, J. Catal. 248 (2007) 175–187.
[38] L. Ilieva, G. Pantaleo, J.W. Sobczak, I. Ivanov, A.M. Venezia, D. Andreeva, Appl. Catal. B: Environ. 76 (2007) 107–114.
[39] C. Gennequin, M. Lamallem, R. Cousin, S. Siffert, F. Aïssi, A. Aboukaïs, Catal. Today 122 (2007) 301–306.
[40] P. Haider, J.-D. Grunwaldt, R. Seidel, A. Baiker, J. Catal. 250 (2007) 313–323.

[41] S. Barison, M. Battagliarin, S. Daolio, M. Fabrizio, E. Miorin, P.L. Antonucci, S. Candamano, V. Modafferi, E.M. Bauer, C. Bellitto, G. Righini, Solid State Ionics 177 (2007) 3473–3484.
[42] W.-C. Li, M. Comotti, A.-H. Lu, F. Schüth, Chem. Commun. (2006) 1772–1774.
[43] H. Provendier, C. Petit, J.-L. Schmitt, A. Kiennemann, C. Chaumont, J. Mater. Sci. 34 (1999) 4121–4127.
[44] S. Ivanova, C. Petit, V. Pitchon, Appl. Catal. A: Gen. 267 (2004) 191–201.
[45] I. Dobrosz, I. Kocemba, J.M. Rynkowski, Pol. J. Environ. Stud. 15 (6A) (2006) 32–36.
[46] M.I. Szynkowska, E. Lesniewska, J. Rogowski, J. Grams, T. Paryjczak, Pol. J. Environ. Stud. 14 (Suppl. IV) (2005) 191–194.
[47] I. Kocemba, Przem. Chem. 3 (82) (2003) 142–145.
[48] S. Huang, L. Li, J. Vleugels, P. Wang, O. van der Biest, J. Eur. Ceram. Soc. 23 (2003) 99–106.
[49] W. Mista, T. Raiment, J. Hanuza, L. Macalik, Mater. Sci.-Pol. 22 (2) (2004) 153–170.
[50] M. Yashima, H. Arashi, M. Kakihana, M. Yoshimura, J. Am. Ceram. Soc. 77 (1994) 1067–1071.
[51] J.Z. Shyu, W.H. Weber, C.R. Peters, R. Usmen, J. Phys. Chem. 92 (1988) 4964–4970.
[52] L. Ilieva, J.W. Sobczak, J.M. Manzoli, B.L. Su, D. Andreeva, Appl. Catal. A: Gen. 291 (2005) 85–92.
[53] A. Trovarelli, M. Boaro, E. Rocchini, C. de Leitenburg, G. Dolcetti, J. Alloys Compd. 323–324 (2001) 584–591.
[54] J.R. González-Velasco, M.A. Gutiérrez-Ortiz, J.-L. Marc, J.A. Botas, M.P. González-Marcos, G. Blanchard, Appl. Catal. B Environ. 22 (1999) 167–178.
[55] M. Boaro, C. de Leitenburg, G. Dolcetti, A. Trovarelli, J. Catal. 193 (2000) 338–347.
[56] S. Ivanova, V. Pitchon, Y. Zimmermann, C. Petit, Appl. Catal. A: Gen. 298 (2006) 57–64.
[57] S. Ivanova, V. Pitchon, C. Petit, J. Mol. Catal. A: Chem. 256 (2006) 278–283.
[58] J.P. Brunelle, Pure Appl. Chem. 50 (1978) 1211–1229.
[59] M.E. Manríquez, T. López, R. Gómez, J. Navarrete, J. Mol. Catal. A: Chem. 220 (2004) 229–237.
[60] S. Ivanova, V. Pitchon, C. Petit, H. Herschbach, A. van Dorsselear, E. Leize, Appl. Catal. A: Gen. 298 (2006) 203–210.
[61] I. Dobrosz-Gómez, I. Kocemba, J.M. Rynkowski, in preparation.
[62] A. Trovarelli, Catal. Rev. Sci. Eng. 38 (1996) 439–520.
[63] Y.-M. Kang, B.-Z. Wan, Catal. Today 35 (1997) 379–392.
[64] A. Venugopal, M.S. Scurrell, Appl. Catal. A: Gen. 258 (2004) 241–249.
[65] L. Ilieva, D. Andreeva, A. Andreev, Thermohim. Acta 292 (1997) 169–174.
[66] H.-W. Jen, G.W. Graham, W. Chun, R.W. McCabe, J.-P. Cuif, S.E. Deutsch, O. Touret, Catal. Today 50 (1999) 309–328.
[67] F.B. Passos, E.R. de Oliveira, L.V. Mattos, Fabio B. Noronha, Catal. Today 101 (2005) 23–30.
[68] S. Salasc, V. Perrichon, M. Primet, M. Chevrier, N. Mouaddib-Moral, J. Catal. 189 (2000) 401–409.
[69] J.A. Wang, T. López, X. Bokhimi, O. Novaro, J. Mol. Catal. A: Chem. 239 (2005) 249–256.
[70] Q. Fu, H. Saltsburg, M. Flytzani-Stephanopoulos, Science 301 (2003) 935–938.
[71] S. Scirè, M. Minicò, C. Crisafulli, C. Satriano, A. Pistone, Appl. Catal. B: Environ. 40 (2003) 43–49.
[72] J. Guzman, S. Carrettin, A. Corma, J. Am. Chem. Soc. 127 (2005) 3286–3287.
[73] J.-D. Grunwaldt, C. Kiener, C. Wögerbauer, A. Baiker, J. Catal. 181 (1999) 223–232.
[74] M. Okumura, S. Nakamura, S. Tsubota, T. Nakamura, M. Azuma, M. Haruta, Catal. Lett. 51 (1998) 53–58.
[75] D.A.H. Cunningham, W. Vogel, H. Kageyama, S. Tsubota, M. Haruta, J. Catal. 177 (1998) 1–10.